

Interannual variations in satellite-sensed vegetation index data from 1981 to 1991

R. B. Myneni,¹ C. J. Tucker,² G. Asrar,³ and C. D. Keeling⁴

Abstract. Normalized difference vegetation index (NDVI) data processed from measurements of advanced very high resolution radiometers (AVHRR) onboard the afternoon-viewing NOAA series satellites (NOAA 7, 9, and 11) were analyzed for spatial and temporal patterns comparable to those observed in atmospheric CO₂, near-surface air temperature, and sea surface temperature (SST) data during the 1981–1991 time period. Two global data sets of NDVI were analyzed for consistency: (1) the land segment of the joint NOAA/NASA Earth Observing System AVHRR Pathfinder data set and (2) the Global Inventory Monitoring and Modeling Studies AVHRR NDVI data set. The impact of SST events was found to be confined mostly to the tropical latitudes but was generally dominant enough to be manifest in the global NDVI anomaly. The vegetation index anomalies at latitudes north of 45°N were found to exhibit an increasing trend. This linear trend corresponds to a 10% increase in seasonal NDVI amplitude over a 9 year period (1981–1990). During the same time period, annual amplitude in the record of atmosphere CO₂ measured at Point Barrow, Alaska, was reported to have increased by about 14%. The increase in vegetation index data between years was especially consistent through the spring and early summer time periods. When this increase was translated into an advance in the timing of spring green-up, the measure (8 ± 3 days) was similar to the recently published estimate of about 7 days in the advance of the midpoint of CO₂ drawdown between spring and summer at Point Barrow, Alaska. The geographical distribution of the increase in vegetation activity was consistent with the reported patterns in springtime warming and decline of snow cover extent over the northern hemisphere land area.

1. Introduction

Station records of near-surface air temperature from the past 30–35 years show a pattern of distinct warming during the winter and springtime periods over the subpolar land area of Alaska, northwestern Canada, and northern Eurasia, especially around Lake Baikal [Chapman and Walsh, 1993]. About 50% of the observed increase in temperature from 1973 to 1992 during the spring months of April and May was found to be related to the decline in snow cover extent [Groisman *et al.*, 1994a]. The global carbon cycle has apparently responded to the recent warm pulse; the amplitude of seasonal CO₂ cycle in the northern hemisphere increased on an average by about 30% since the early 1960s, indicating increased biospheric activity at these latitudes [Keeling *et al.*, 1996]. Interestingly, the midpoint in atmospheric CO₂ drawdown between spring and summer was found to be advanced by about 7 days, which Keeling *et al.* interpret as an indication of longer growing season. Our analyses of two satellite-sensed vegetation index data sets appear to confirm the results of Keeling *et al.* [1996]. The vegetation index data indicate a significant greening trend from increasing seasonal amplitude and growing season dura-

tion in the northern high latitudes. These and various other results are reported in this paper. The article is organized as follows: after a brief description of the data sets (section 2) and methods (section 3), interannual variations in large area averages are discussed (section 4), followed by the observed trends in the northern high latitudes (section 5) and concluding remarks (section 6).

2. Pathfinder AVHRR NDVI Data Set

2.1. NDVI

A data set of normalized difference vegetation index (NDVI) at 8 km resolution (square pixels) was produced with data from the advanced very high resolution radiometers (AVHRR) onboard the afternoon-viewing NOAA series satellites (NOAA 7, 9, and 11) under the joint sponsorship of NASA and NOAA Earth Observing System Pathfinder project [James and Kalluri, 1994]. The data processing included improved navigation, intersatellite calibration, and correction for Rayleigh scattering.

The normalized difference vegetation index (NDVI) is defined as the ratio

$$\frac{\text{channel 2 reflectance} - \text{channel 1 reflectance}}{\text{channel 2 reflectance} + \text{channel 1 reflectance}}$$

where channel 1 is the 580–680 nm wavelength band (red band) and channel 2 is the 725–1100 nm wavelength band (near-infrared band). The NDVI is expressed on a scale from –1 to 1. For green vegetated surfaces, near-infrared reflectance is always greater than red reflectance, and therefore NDVI > 0. Seasonal averages of Pathfinder NDVI data tend

¹Department of Geography, Boston University, Boston, Massachusetts.

²Biospheric Sciences Branch, NASA Goddard Space Flight Center, Greenbelt, Maryland.

³Mission to Planet Earth, NASA Headquarters, Washington, D. C.

⁴Scripps Institute of Oceanography, La Jolla, California.

to be slightly negative or close to zero for bare areas (e.g., Sahara in Africa and Taklimakan in China) and saturate at about 0.65 NDVI for dense forested landscapes. The utility of NDVI data for studies on global vegetation dynamics has been well documented [Tucker *et al.*, 1985, 1986, 1991]. NDVI data are generally found to be well correlated to the fraction of photosynthetically active radiation (400–700 nm) absorbed by green vegetation [Asrar *et al.*, 1984]. Its time integral is a good predictor of biomass production [Tucker, 1980; Prince, 1991] and carbon fixation [Fung *et al.*, 1987]. In fact, it can be rigorously shown using radiative transfer theory that NDVI is indicative of the abundance and activity of leaf chlorophyll pigments [Myneni *et al.*, 1995]. A history of the use of AVHRR data for land applications can be found in the work of Tucker [1996].

2.2. Compositing

Complete coverage of the land surface is possible daily with AVHRR sensors. The daily data can be of poor quality because of atmospheric conditions (clouds and aerosols). Therefore the daily data are composited; that is, a month is divided into three compositing periods: days 1–10 are compositing period 1, days 11–20 are compositing period 2, and days 21 to the end of the month are compositing period 3. The maximum NDVI value during each compositing period is chosen to represent that compositing time period, because atmospheric effects almost always tend to decrease the magnitude of NDVI [Holben, 1986]. Correction for atmospheric effects requires information on atmospheric gases, aerosols, clouds and surface scattering properties [Tanrè *et al.*, 1992], and is beyond the scope of current state of art. One unfortunate consequence of maximum-value compositing is the retention of bad scan lines. For example, if channel 1 reflectance value is corrupted, $NDVI \approx 1$, and this value will be retained. Bad scan lines were found in the Pathfinder NDVI data set, although very infrequently. The three 10 day NDVI composite values in a month were averaged to obtain a monthly NDVI value, which was then used in the analysis reported here.

2.3. Known Problems With the Data Set

The reported solar zenith angles were found to be in error (less than 5° maximum). NDVI is not affected by inaccuracies in solar zenith angle, but caution is required when using the individual channel reflectances (channel data were not used in this study). Only a partial correction for Rayleigh scattering was implemented. This correction is likely to contain a small error because of incorrect solar zenith angles. Details can be found in the current version of the data set user manual [Aghu and James, 1994].

3. Preliminary Analysis and Modifications

3.1. Intersensor Variations

Pathfinder NDVI data for the period July 1981 to December 1992 were utilized in this study. The data were collected by three different sensors: (a) NOAA 7 from July 1981 to January 1985, (b) NOAA 9 from February 1985 to October 1988, and (c) NOAA 11 from November 1988 to December 1992. Within the life of a satellite, degradation in data quality results from loss of calibration. Moreover, the drift in orbit results in later and later revisits of the satellite at a given location on the Earth [Price, 1991]. This means that reflectance measurements are made at progressively higher solar zenith angles which consid-

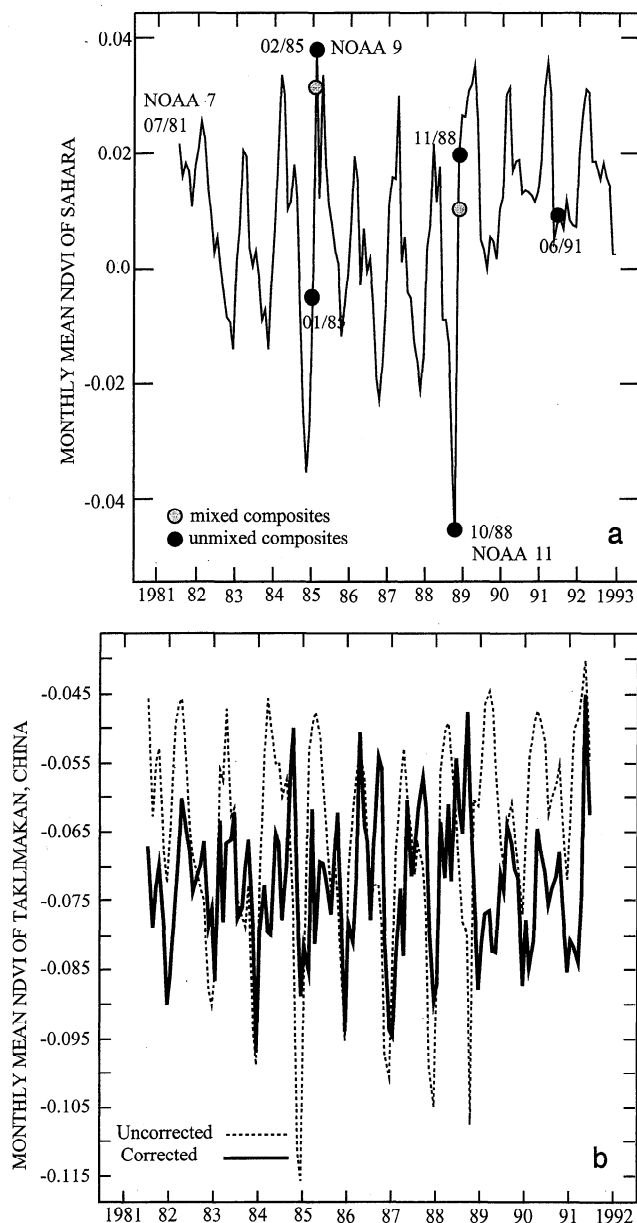


Figure 1. (a) Time series of monthly normalized difference vegetation index (NDVI), spatially averaged over a large region in the hyperarid part of Sahara, plotted to show intrasensor and intersensor variations over a supposedly invariant target. (b) A similar time series (dashed line) for Taklimakan, China. A simple ad hoc correction is to subtract the monthly NDVI signal of the Sahara (Figure 1a); the result is plotted as a solid line in Figure 1b.

erably increase the atmospheric effect. Pathfinder data processing corrects for these effects by recalibrating the data using time-dependent gains, offsets, and invariant ground targets of known properties [James and Kalluri, 1994; Rao and Chen, 1995].

An assessment of the Pathfinder data set can be made by plotting the monthly NDVI time series of a desert target. A large region in the hyperarid part of Sahara (about 20°N) of about $1.42 \times 10^6 \text{ km}^2$ area (22,154 pixels) was selected for this purpose. This time series, shown in Figure 1a, exhibits (1) cyclical annual variation due to the movement of the Sun, (2)

data quality problems during the last months of NOAA 7 and NOAA 9, and (3) NOAA 11 data to be of slightly higher magnitude than NOAA 7 and NOAA 9. Mixing of data from NOAA 7 (first composite in February 1985) and NOAA 9 (the other two composites) corrupts the monthly average NDVI of February 1985 slightly. The same is true of November 1988, when data from NOAA 9 and NOAA 11 were mixed. The eruption of Mount Pinatubo in June 1991 injected a significant amount of aerosols into the stratosphere. The obscuration effect is not evident here (but see below; compare Figure 3a).

3.2. Saharan Correction

From an intuitive and theoretical point of view, one would expect that an index such as NDVI, an indicator of vegetation density and photosynthetic capacity, should be close to zero and nearly time invariant over deserts. Indeed, the NDVI data set of Africa (the Global Inventory Monitoring and Modelling Studies (GIMMS) data set) used by *Tucker et al.* [1994] to study the expansion and contraction of the Sahara shows this characteristic. With this in mind, the Saharan time series shown in Figure 1a was used as an offset throughout this analysis; that is, the monthly NDVI of Sahara was subtracted from the monthly NDVI of each pixel. The effect of this correction on the time series of monthly NDVI of a hyperarid region in China (Taklimakan) is shown in Figure 1b. The uncorrected signal (Pathfinder data) clearly shows both intrasensor and intersensor variations. A partial correction for these quality problems can be accomplished, if the Saharan time series is used as an offset. A more rigorous correction would require recalibration of the daily channel data and re-compositing the corrected NDVI data. Such an effort is beyond the scope of this work and available resources.

AVHRR NDVI data have been used to monitor the average seasonal greenness of the 200–400 mm precipitation zone in the Sahel by *Tucker et al.* [1991, 1994]. Their data were corrected to remove soil background contribution to NDVI; the data from August 1991 to December 1992 data were also corrected for Pinatubo aerosol obscuration. The Pathfinder data did not have these corrections. The seasonal greenness in this region varies substantially from year to year, and its determination requires highly accurate data. Therefore their results provide an opportunity to benchmark the Pathfinder data set. The Pathfinder data when compared to *Tucker et al.*'s [1994] results show certain discrepancies (Figure 2a). For example, their results indicate that seasonal greenness in this zone increased from 1985 to 1986, while the Pathfinder data actually show a decrease. Likewise, they report a decrease in seasonal NDVI from 1988 to 1989, while the Pathfinder data show an increase. However, when the Saharan monthly NDVI, shown in Figure 1a, is used as an offset, the two results match, albeit qualitatively. The average difference between the two data sets, in this case study, is about 0.02 NDVI. This difference in magnitudes may be explained partly by the fact that 10 day composites were averaged to obtain a monthly NDVI in the case of Pathfinder data, while *Tucker et al.* [1994] represented the monthly NDVI as the maximum of two 15 day composites (the former is always lower in magnitude than the latter). The importance of Pinatubo aerosol correction is also evident from this figure. In estimating the North-South movement of the Sahara, *Tucker et al.* [1994] relied on the relationship between Sahelian rainfall and GIMMS NDVI data, which they found to be statistically significant. A similar relationship was also obtained with the Sahara-subtracted Pathfinder NDVI

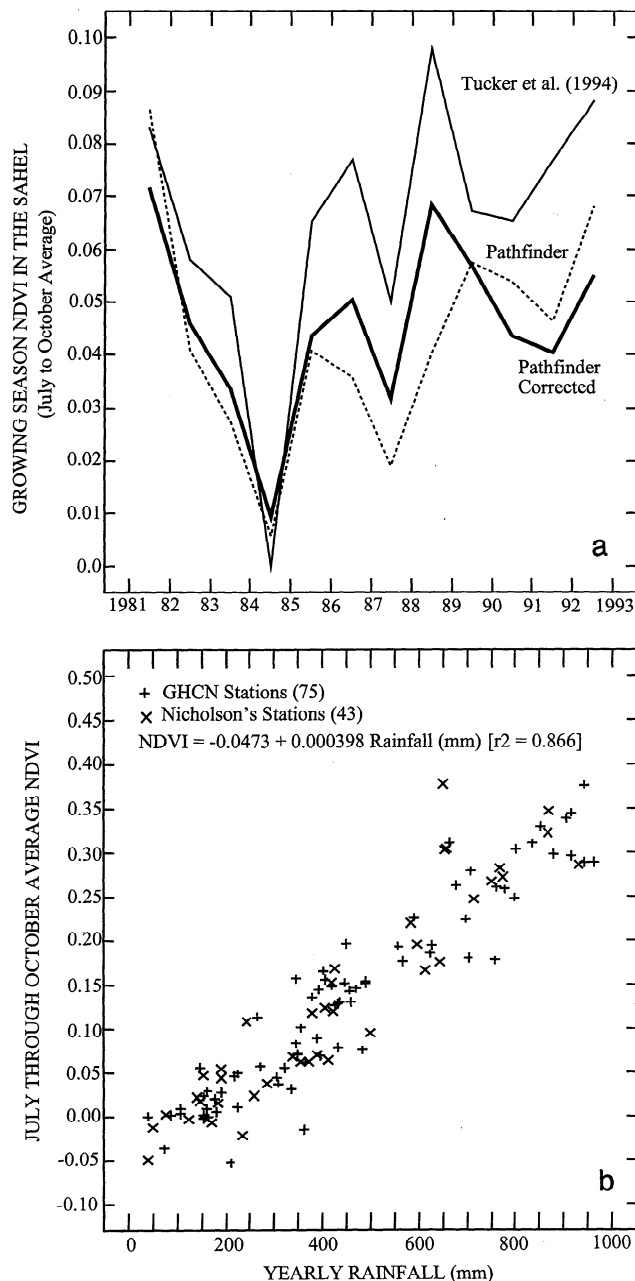


Figure 2. (a) Average growing season NDVI in the 200–400 mm rainfall zone in the Sahel. The growing season is assumed to be from July to October. (b) The relationship between average growing season NDVI and annual rainfall in the Sahel. The GHCN data are from [Voss *et al.*, 1992]. Rainfall data from non-GHCN stations are from Nicholson (personal communication, 1995).

and Sahelian rainfall (Figure 2b), thus further confirming the validity of the Saharan correction of Pathfinder NDVI data set.

3.3. Evaluation of Global NDVI Anomaly

Let $x(k, m, y)$ be the monthly NDVI of pixel k in month m and year y . The monthly NDVI x itself is the average of three 10 day maximum-value NDVI composites. Let $\bar{x}(k, m)$ be the long-term monthly average NDVI of pixel k in month m ,

$$\bar{x}(k, m) = \frac{1}{N_y} \sum_{y=1}^{y=N_y} x(k, m, y), \quad (1)$$

where N_y is the number of years for which the NDVI data are available for pixel k in month m . Monthly NDVI anomaly $x'(k, m, y)$ is evaluated as

$$x'(k, m, y) = [x(k, m, y) - \bar{x}(k, m)]. \quad (2)$$

Spatial averaging of x' requires some care, the specifics of which are discussed in the next section. For the time being it suffices to note that spatial averaging is performed over those pixels which meet the following two conditions: (1) the long-term monthly average NDVI of a pixel \bar{x} is greater than 0.1 NDVI and (2) its standardized anomaly $x'_s(k, m, y) < |3\sigma|$. Here x'_s is defined as

$$x'_s(k, m, y) = \frac{[x(k, m, y) - \bar{x}(k, m)]}{\sigma(k, m)}, \quad (3)$$

where $\sigma(k, m)$ is the long-term monthly NDVI standard deviation of pixel k in month m ,

$$\sigma(k, m) = \left\{ \frac{1}{N_y - 1} \sum_{y=1}^{y=N_y} [x(k, m, y) - \bar{x}(k, m)]^2 \right\}^{0.5}. \quad (4)$$

Anomalies evaluated in this manner and inferences about trend drawn from these are seasonally dependent (also, related discussion by Thomson [1995]).

The globally averaged monthly NDVI anomaly, $\langle x' \rangle(m, y)$, is shown in Figure 3a for four cases: (1) Pathfinder data from July 1981 to December 1992, (2) Pathfinder data from July 1981 to December 1992 with Saharan correction, (3) same as in case 2 but with a simple correction for Pinatubo aerosols derived from the GIMMS African data set for the time period August 1991 to December 1992, and (4) same as in case 2 but only for the time period July 1981 to June 1991, i.e., without the data after the Mount Pinatubo eruption in June 1991. The Saharan correction helps contain the sharp decrease in NDVI anomaly toward the end of NOAA 7 (late 1984/early 1985) and NOAA 9 (fall 1988). Also, the dramatic increase in NOAA 11 anomalies are somewhat damped. It will be seen that NOAA 11 data are generally of higher magnitude, and the Saharan correction helps correct for some of the problems with intersensor variations (next section).

The decrease in the global NDVI anomaly from spring 1991 onward coincided with the 1991–1992 El Niño event and the eruption of Mount Pinatubo. The dramatic decrease in the NDVI anomaly during this rather weak El Niño, when compared to the 1982/1983 El Niño (the strongest this century), leads one to conclude that the simple correction for Pinatubo aerosols is questionable. Therefore only the Sahara-subtracted Pathfinder NDVI data from the beginning of the record till the eruption of Mount Pinatubo (July 1981 to June 1991) were utilized for the remainder of this study.

These results highlight the need to apply the so-called Saharan correction to account for intrasensor and intersensor variations. A question of some interest is how does this correction change the data set? The power spectra of the global NDVI anomaly calculated with the uncorrected and corrected Pathfinder data are shown in Figure 3b. The correction exposes a peak in the spectrum at a period of 43 months, indicating the El Niño Southern Oscillation (ENSO) signal in the data [Myneni et al., 1996]. In the uncorrected data the ENSO signal may have been partly obscured by intersensor variations; NOAA 7, 9, and 11 record lengths were 42, 46, and 50 months, respectively. The spectrum of uncorrected data shows a sharp

peak at a period of 21 months and a smaller peak at a period of 16 months. The correction dampens the 21 month oscillation and broadens it to a span of 18–21 months, reasons for which are not clear. Recent studies indicate that the tropospheric quasi-biennial oscillation may play an important role in the timing and strength of ENSO [Alexander and Weickmann, 1995]. Such biennial oscillations were also observed in CO₂ amplitude records recently [Keeling et al., 1996]. Therefore a quasi-biennial oscillation may be expected in NDVI anomaly data, but the period is shorter.

3.4. Distribution of Anomalies About the Mean

A question of interest regarding the distribution of anomalies with respect to the standard deviation is the following: how does the global NDVI anomaly change if it were to be evaluated successively from anomalies increasingly away from the mean? This is shown in Figure 3c. For example, the $|1 - 2|\sigma$ global NDVI anomaly refers to spatially averaging monthly NDVI anomalies $x'(k, m, y)$ over only those pixels with standardized monthly NDVI anomalies $x'_s(k, m, y)$ between $|1 - 2|\sigma$. It is clear from Figure 3c that farther away from the mean, the anomalies are generally negative; that is, the sum

$$\langle \bar{x}' \rangle (|1 - 2|\sigma) = \sum_{m=1}^{m=12} \sum_{y=1}^{y=N_y} \langle x' \rangle(m, y),$$

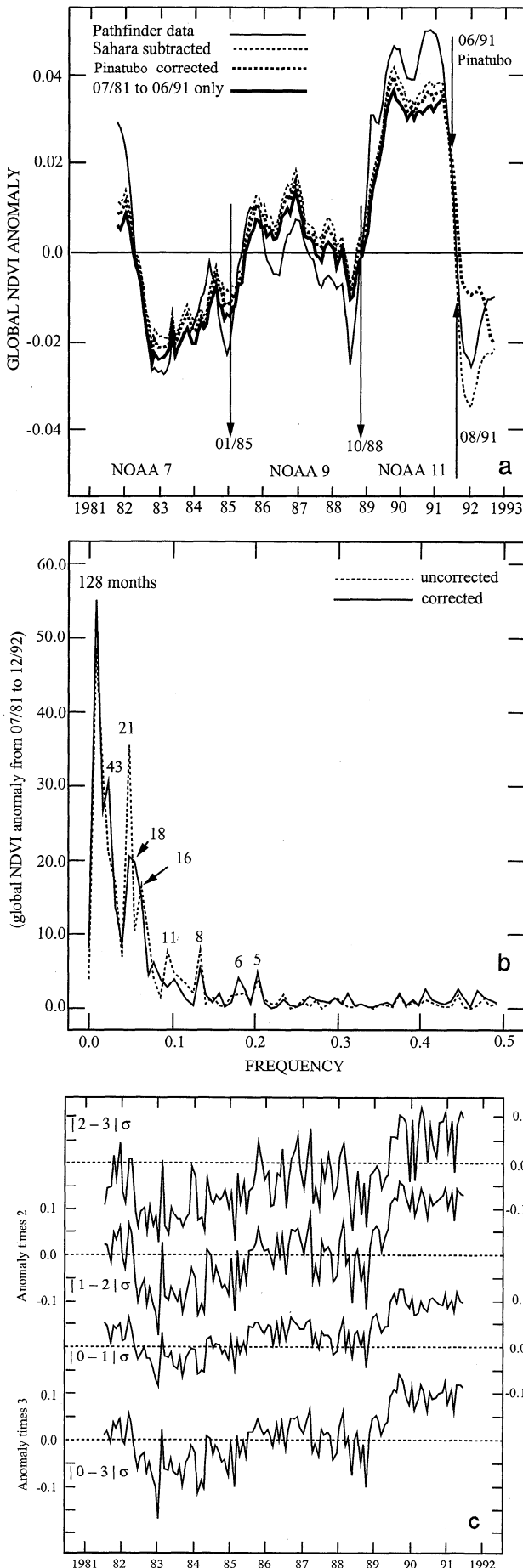
$$x'_s(k, m, y) \in |1 - 2|\sigma$$

is negative and is greater than $\langle \bar{x}' \rangle (|2 - 3|\sigma)$. One would expect these sums to be close to zero, if the anomalies were distributed evenly on the positive and negative sides of the mean. Because the sum $\langle \bar{x}' \rangle (|0 - 3|\sigma)$ is almost zero (it is not exactly zero because those pixels with $x'_s(k, m, y) > |3\sigma|$ are treated as outliers and not included in spatial averages), it is concluded that in general the number of pixels showing positive NDVI anomalies is greater than those showing negative NDVI anomalies. This means that the average negative NDVI anomaly is larger in magnitude than the positive NDVI anomaly. This is not surprising for the following two reasons: (1) almost all deleterious effects (namely, atmospheric effects) tend to diminish NDVI, and (2) NDVI initially increases almost linearly with vegetation amount and then tends to an asymptotic value over dense vegetation. Therefore it is more difficult to observe any systematic increases in NDVI anomalies than decreases, when such anomalies are spatially averaged and analyzed for their temporal evolution. This viewpoint is especially noteworthy, for precisely such a systematic increase in NDVI is observed in the northern high latitudes (following sections).

4. Spatial Averages

4.1. Global Averages

What is the average NDVI of the globe or any land area of substantial spatial extent? The answer depends on the method used to identify vegetated areas (as opposed to nonvegetated areas such as exposed soils, snow, etc.), such that spatial averaging is performed only over the vegetated areas to obtain an unbiased estimate of spatially averaged NDVI. There is, of course, no objective way of defining, in terms of NDVI data, when a pixel is vegetated or bare, because it invariably requires the subjective use of a threshold NDVI value. Several methods



of spatial averaging can be devised, each with a different purpose, but none ideal, as the following discussion will show.

Let $x(k, m, y)$ be the monthly NDVI of pixel k in month m and year y . Note that the monthly NDVI x itself is the average of three 10 day composites. Let $\bar{x}(k, m)$ be the long-term monthly average NDVI of pixel k in month m (equation (2)). Let $x'_s(k, m, y)$ be the standardized monthly NDVI anomaly (equation (3)) and $\langle x \rangle(m, y)$ be the spatially averaged monthly NDVI. A threshold NDVI value of 0.1 is used in the following analysis. This arbitrary value reflects our understanding of the Pathfinder data set and NDVI values generally seen in the transition zones between deserts and vegetated areas (compare Figure 2a).

Vegetated pixels may be identified with either of the two following definitions: (1) the monthly NDVI $x(k, m, y)$ is greater than the threshold NDVI value and (2) the long-term monthly average NDVI $\bar{x}(k, m)$ is greater than the threshold NDVI value, and the monthly standardized NDVI anomaly x'_s is less than 3σ . The validity of these definitions depends only on the threshold NDVI value, and in general, definition 2 is more robust than definition 1.

The spatial extent of averaging requires similar careful considerations. The purpose of evaluating spatial averages is to study temporal variations. These can be of three types: (1) variations that may be considered natural, such as seasonal changes, (2) artificial variations due to sensor degradation with time and/or poor intersensor calibration, and (3) variations due to climate, such as droughts, ENSO, etc. The spatial extent of averaging can be chosen to highlight one of the above variations. For instance, if spatial averaging is performed over those pixels with \bar{x} in August > 0.1 NDVI and x'_s in August $< 3\sigma$, the number of pixels will be constant from month to month and year to year (denoted as CMY). Such a method will highlight NDVI seasonality. On the other hand, if spatial averaging is performed over those pixels with $x(k, m, y) > 0.1$ NDVI, the number of pixels varies from month to month and year to year (denoted as VMY). This method is best suited to characterize intrasensor and intersensor variations in NDVI. Finally, if spatial averaging is performed over pixels with $\bar{x} > 0.1$ NDVI and $x'_s < 3\sigma$, the number of pixels will vary from month to month but is almost constant from year to year during the same month (denoted as VMCY). This method is best suited to the study of climate-induced variations in NDVI. Each of these methods have drawbacks (discussed below), and it should not be construed that a particular method will suppress completely all other variations and highlight those that it is intended to.

4.1.1. Method A (II-CMY). This is the simplest of the four methods considered here. A pixel is considered vegetated if \bar{x} in August > 0.1 NDVI and x'_s in August $< 3\sigma$. August is chosen because it is the greenest month of the year with a global vegetated area of about $100 \times 10^6 \text{ km}^2$, or about 1.57×10^6 square pixels of side 8 km (Figure 4a). The advantage of this method is that it highlights the seasonality in spatially

Figure 3. (opposite) (a) Time series of global NDVI anomaly evaluated from Pathfinder data with and without Saharan and Pinatubo corrections. (b) Power spectra of global NDVI anomaly calculated with the Sahara-uncorrected and corrected Pathfinder data. (c) Time series of global NDVI anomalies evaluated selectively from data spaced, in units of standard deviation, away from the mean.

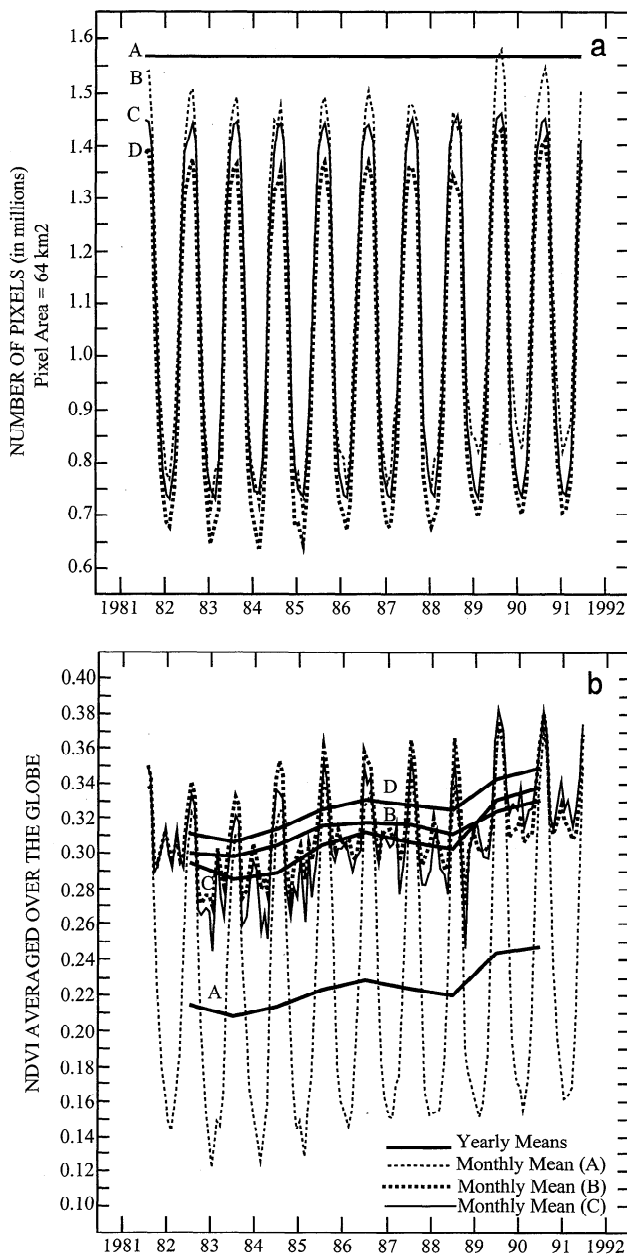


Figure 4. Characteristics of the four methods of spatial averaging described in the text: (a) number of pixels used in evaluating spatial averages, (b) monthly and yearly average NDVI of the globe.

averaged NDVI time series. The disadvantage of this method is that deciduous pixels in the southern hemisphere with long-term August NDVI values less than the threshold but are green during the austral summer season are not considered in the process of spatial averaging.

4.1.2. Method B (I-VMY). In this method, spatial averaging is performed over all pixels with $x > 0.1$ NDVI. The number of pixels $N_p(m, y)$ used to evaluate $\langle x \rangle(m, y)$ changes from month to month and year to year (Figure 4a). This can lead to biased estimates of $\langle x \rangle$ especially when intersensor calibration is poor. For instance, NOAA 11 NDVI data are seen to be generally higher in magnitude than NOAA 7 and NOAA 9, even after subtracting the Sahara signal. Therefore the number of pixels with a monthly NDVI value greater than

0.1 increases (Figure 4a), which also coincided with the period when NDVI increased globally!

4.1.3. Method C (II-VMCY). In this method, spatial averaging is performed over those pixels with $\bar{x} > 0.1$ NDVI and $x'_s < |3|\sigma$. The number of pixels N_p in a given month is nearly constant from year to year (nearly but not exactly constant because even though $\bar{x}(k, m)$ is evaluated from the entire record, rejection of outliers, while spatially averaging as required by $x'_s(k, m, y) < |3|\sigma$, changes $N_p(m, y)$ from year to year for the same month). Therefore $\langle x \rangle$ is estimated from nearly the same sample of locations interannually (Figure 4a). For instance, if $x(k, m, y) < 0.1$, but $\bar{x}(k, m) > 0.1$, and $x'_s(k, m, y) < |3|\sigma$, it is treated as a vegetated pixel and is included in the spatial average. On the other hand, if $x(k, m, y) > 0.1$, but $\bar{x}(k, m) < 0.1$, the pixel is considered non-vegetated, as it should be because the long-term monthly average NDVI \bar{x} is a more reliable indicator than the instantaneous measurement x (but see case 2 below). This is a valuable attribute when working with data from different sensors. Therefore the vegetated locations are fixed on the basis of the entire record of data, and changes in NDVI from month to month and year to year are captured in $\langle x \rangle$. The disadvantages of this method are as follows: (1) the long-term mean will be biased if intersensor alignment is poor and (2) the greening of an otherwise bare pixel is ignored.

4.1.4. Method D (I, II-VMY). In this method, spatial averaging is performed over those pixels with x and $\bar{x} > 0.1$ NDVI, and $x'_s < |3|\sigma$. Here the disadvantages of method B are retained, namely sensitivity to the threshold, and the advantage of method C is lost, namely the utility of long-term monthly average NDVI. Thus the number of pixels N_p changes from year to year in the same month and is generally smaller than in methods B and C (Figure 4a). The number of pixels, especially with NDVI values about the threshold, determines the merit of an average. For instance, if the threshold is reduced to 0.05 NDVI, N_p would increase significantly because of large deserts in Africa and Asia, thus resulting in an unrealistic estimate of globally averaged NDVI.

4.1.5. Global NDVI. The monthly and yearly average NDVI of the globe evaluated according to the four methods of spatial averaging discussed above are shown in Figure 4b. All four methods resulted in a systematic increase in the yearly average NDVI of the globe; 2.0, 1.2, 2.0, and 1.6% per year from 1982 to 1990 or about 10–16% over the 8 year period of the record. The linear regressions are statistically significant even if NOAA 11 data (1989 and 1990) are excluded. The corresponding results are 1.0, 1.0, 1.1, and 1.2% increase in yearly average NDVI or about 6–7% over the 6 year period (1982 to 1988). During the 9 year period from 1981 to 1990, annual amplitude of the seasonal CO₂ cycle increased by about 14% at Point Barrow in Alaska [Keeling *et al.*, 1996]. At this juncture it is important to note the limitations of regression analysis on short samples of data, i.e., the determination of a trend in the presence of low-frequency variations due perhaps to SST oscillation events, soil moisture fields, etc. The connection between observed increases in CO₂ amplitude, springtime surface air temperatures, and seasonal NDVI is discussed later.

4.2. Averages by Latitude

Time series of NDVI for different latitudinal bands and for the whole globe are shown in Figure 5a. Spatial averaging was performed according to Method A described previously, to

explicitly show seasonality in the extratropics. At latitudes north of 45°N the winter time NDVI is close to zero. Therefore the NDVI value during the summer time (July and August) is a good surrogate for the amplitude in these latitudes. The yearly average NDVI shows an increase both globally and latitudinally (significantly in the higher northern latitudes), except at latitudes south of 15°N. When NOAA 11 data (1989 and 1990) are not included, the increase in yearly NDVI is somewhat less but still significant. It should be emphasized that these linear trend estimates are specific to the method of spatial averaging. If method B, C, or D was used, the linear trend estimates would either be lower (with NOAA 11 data) or nearly unchanged (without NOAA 11 data). In view of (1) the subjectivity regarding spatial averaging, (2) residual problems in NDVI data (the data were not rigorously atmosphere-corrected, intersensor linkage artifacts, etc.), and (3) the short timescale, we emphasize only the qualitative nature of the trend (i.e., an increase or a decrease) rather than its magnitude. This caveat must be kept in mind for the remainder of this work.

The time series of the total NDVI anomaly evaluated according to method C is shown in Figure 5b. Spatial totals, rather than averages, are shown because the number of pixels in the far extratropics that satisfy the criteria required for inclusion in spatial calculations, namely $\bar{x}(k, m) > 0.1$ and $x'_s(k, m, y) < |3|\sigma$, is fewer during wintertime; thus biasing the averages. The relative contribution of these five latitudinal bands to the total NDVI anomaly of the globe can also be seen in Figure 5b, which is another reason why spatial totals are more informative than averages. Two observations can be made: (1) the time series of global NDVI anomaly resembles the time series in the tropics (15°S–15°N), the interannual variability of which is strongly influenced by the El Niño Southern Oscillation phenomenon, and (2) the time series of the NDVI anomaly at latitudes north of 45°N clearly shows an increasing trend over the entire period of record.

The NDVI anomaly in the tropics shows a large increase starting from November 1988, which also coincided with the change in satellites from NOAA 9 to NOAA 11. A somewhat smaller increase is seen during the switch from NOAA 7 to NOAA 9 in January 1985, although this increase began in the last months of the NOAA 7 record (and the anomaly north of 45°N actually shows a decrease). This raises a question regarding anomalous variations in NDVI from sensor changes. Although efforts have been made to establish proper intersensor calibration linkages [James and Kalluri, 1994; Rao and Chen, 1995], some residual effects cannot be ruled out, especially between NOAA 9 and NOAA 11. This situation confounds proper interpretation of the tropical NDVI anomaly time series. For instance, intense SST oscillatory events in the tropical Pacific and Atlantic Oceans from 1982 to early 1989 have been linked to decreased vegetation growth in large regions of the semiarid tropics [Myneni et al., 1996]. The increase in tropical and global NDVI anomaly starting from late 1988 also coincided with an unprecedented decline in atmospheric CO₂ anomaly, from a peak value in late 1988 to a minimum in late 1993 [Keeling et al., 1995]. These interpretations, presented below (section 4.3), must be caveated in light of possible sensor change effects.

4.3. Atmospheric CO₂ and NDVI

The 1980s experienced well-defined alternating El Niño Southern Oscillation (ENSO) warm and cold events [Philan-

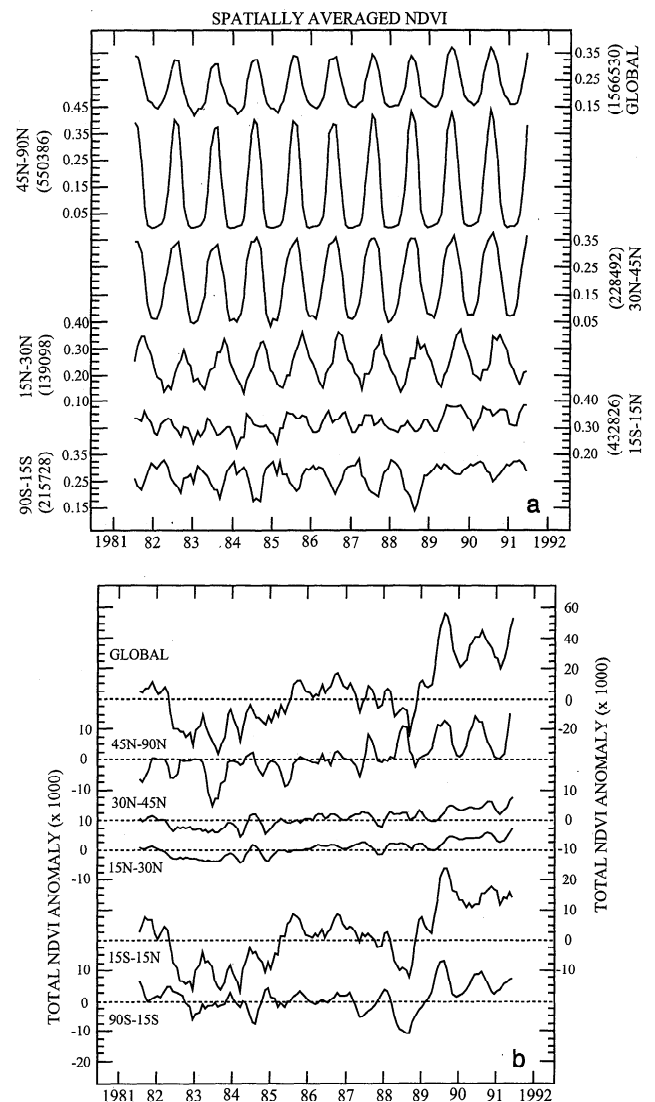


Figure 5. Time series of (a) spatially averaged NDVI and (b) spatially summed NDVI anomaly for coarse latitudinal bands and the whole globe. The number of 8×8 km pixels in each case is also shown in parentheses in Figure 5a.

der, 1990]. Linked NDVI and sea surface temperature (SST) anomaly areas in semiarid (annual rainfall less than 700 mm) regions of Africa, Australia, and South America during the 1982–1990 period have been recently described [Myneni et al., 1996]. It was found that large areas (between 0.5 and 1.5 million km²) in semiarid regions of these continents experienced rainfall anomalies that were directly correlated to SST anomalies in the equatorial Pacific. Although the warm events of the ENSO cycle were associated with decreased rainfall and the cold events with increased rainfall, this pattern was not always consistent, at least during the 1982–1990 time period. For instance, southeastern South America, encompassing regions in southern Brazil, northern Argentina, Paraguay, and Uruguay, experienced a strong drought during the 1988–1989 cold event of the ENSO cycle [Myneni et al., 1996].

A measurable link between atmospheric CO₂ drawdown by vegetation and NDVI dynamics was demonstrated by Tucker et al. [1986]. Interannual variations in observed atmospheric CO₂ and inferred biospheric carbon exchange since 1980 are dis-

cussed by Keeling *et al.* [1995]. These variations are shown in Figure 6a together with the global NDVI anomaly and NINO3 index (SST anomaly in the equatorial Pacific region of 5°S–5°N latitude and 90°W–150°W longitude which characterizes

ENSO cycle warm and cold events). The biosphere is a source of carbon during warm events and a sink during cold events [Keeling *et al.*, 1995]. The atmospheric CO₂ anomaly, with respect to a 20 year baseline period (1959–1979), increased from 1980 to late 1988 and from then onward decreased [Keeling *et al.*, 1995]. The global NDVI anomaly, which is indicative of photosynthetic carbon fixation by plants, was mostly negative during the period of increasing atmospheric CO₂ anomaly, and starting from late 1988, it was positive till mid-1991, when the eruption of Mount Pinatubo corrupted the satellite data.

While the 1980s experienced well-defined SST oscillation events both in the equatorial Pacific and in the tropical Atlantic [Philander, 1986], the situation during the 1990–1995 time period was different. There were three weak warmings in the equatorial Pacific beginning from early 1991 onward. The strong covariation between biospheric carbon exchange and NINO3 index, observed in the 1980s, appears weakened from early 1991 onward. The decrease in atmospheric CO₂ anomaly from the time of Mount Pinatubo eruption in mid-1991 till late 1993 was uncharacteristically sharp [Keeling *et al.*, 1995]. Although air temperatures decreased after the Mount Pinatubo eruption, the global anomaly is still high, about 0.3°C [Jones *et al.*, 1994], and 1995 was the warmest year so far [Anonymous, 1996]. When the satellite data are corrected for stratospheric aerosol obscuration, these issues can be further studied.

The autocorrelation functions of these time series for the July 1981 to June 1991 time period are shown in Figure 6b. The similarity between the autocorrelation functions (acfs) of atmospheric CO₂ anomaly and NDVI anomaly is intriguing. So is the striking similarity between the acfs of NINO3 index and biospheric carbon exchange, as previously noted and discussed by Keeling *et al.* [1995]. Further interpretation is hampered by the fact that the standard error (SE) of an acf estimate at a lag increases with lag, and estimates within $|1|$ or $|2|$ SE must be treated as identical to zero. The cross-correlation function indicates that the biospheric carbon exchange tends to lag NINO3 index by about 6 months (plot not shown). The cross-correlation function (ccf) of NDVI anomaly versus atmospheric CO₂ anomaly is highest at zero lag (0.4) and reaches a minimum at a lag of about 65 months (–0.4). This correlation reversal corresponds to a similar reversal in the acfs of the corresponding quantities (Figure 6b) but at a higher lag (80–90 lags). This can be traced to increasing atmospheric CO₂ anomaly and decreasing NDVI anomaly from mid-1981 to late 1988. Thereafter, the trends reverse (Figure 6a).

Variability in a time series can be studied by evaluating the structure function

$$S_q(k) = \frac{1}{N-k} \sum_{t=1}^{N-k} |x(t+k) - x(t)|^q, \quad (5)$$

where k is the distance between two observations in a time

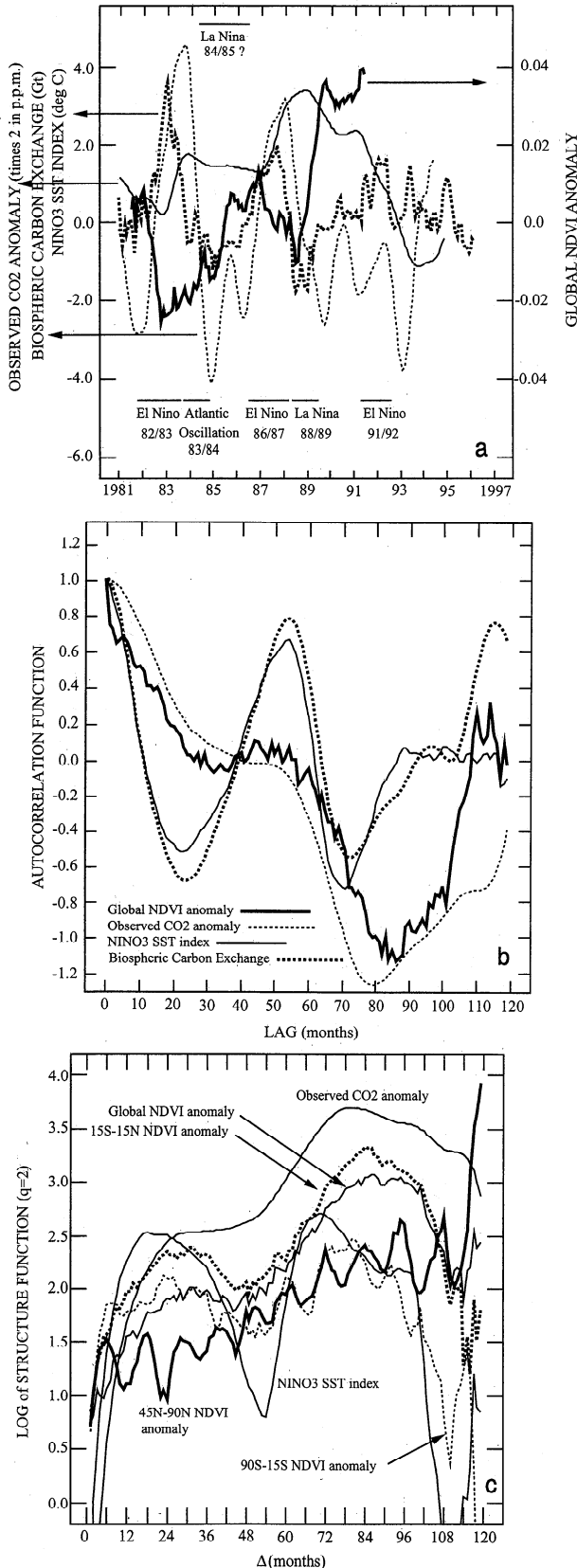


Figure 6. (opposite) (a) Time of series of global NDVI anomaly, atmospheric CO₂ anomaly [Keeling *et al.*, 1995], inferred biospheric carbon exchange [Keeling *et al.*, 1995], and NINO3 sea surface temperature index [Woodruff *et al.*, 1993]. (b) Autocorrelation functions of global NDVI anomaly, atmospheric CO₂ anomaly, inferred biospheric carbon exchange, and NINO3 sea surface temperature index. (c) Structure functions of global and latitudinal NDVI anomalies, atmospheric CO₂ anomaly, and NINO3 sea surface temperature index. The value of 2 for q was chosen because of the resulting similarity with power spectra.

series and q can be used to focus on the scale of variations of interest. As k approaches N , confidence in the estimate of S decreases. The structure functions of NINO3 SST index, atmospheric CO_2 anomaly, and NDVI anomaly for the globe and for different latitudinal bands are shown in Figure 6c. The structure function of NINO3 SST index exhibits a secondary minimum at a distance of about 55 months, which corresponds to the secondary maximum in its acf (Figure 6b). This reflects the combined duration of a warm and cold event during the 1980s. Variability at a similar scale is also observed in the structure function of NDVI anomalies at latitudes south of 15°N . The similarity between the structure functions of global NDVI anomaly and atmospheric CO_2 anomaly should be noted. Both show the impact of ENSO cycle events, albeit faintly. Most striking, however, is the variability in the time series of NDVI anomaly at latitudes north of 45°N , which clearly shows the increasing trend.

5. Increased Seasonal Greenness in High Latitudes

It will be noted from previous discussion that the time series of spatially averaged monthly NDVI and spatially summed monthly NDVI anomalies (Figures 5a and 5b) show a linear trend over the entire period of record (July 1981 to June 1991) at latitudes north of 45°N . This trend is in contrast to the variability seen at other latitudes, especially in the tropics. The linear trend in the northern high latitudes is discussed below in terms of (1) the average growing season NDVI, (2) seasonal NDVI amplitude, and (3) length of the growing season. Growing season in the following discussion must be understood as the active growing season, i.e., the period during which photosynthesis actually occurs, as opposed to the conventional concept of growing season, measured, for example, in degree days.

5.1. Average Growing Season NDVI

A characteristic feature of temporal profiles of NDVI at locations in the northern high latitudes (latitudes north of 35°N) is the seasonality (Figure 7). NDVI integrated over the growing season may be conceptualized as an area, with amplitude and growing season duration representing the two dimensions. Increase in one (assuming the other does not decrease) or both of the dimensions should increase this area. This area can be reasonably well approximated by total NDVI at a location between the months of May to September. This is an approximation because the actual growing season duration decreases with increase in latitude. Seasonality in NDVI is such that it peaks during the months of June, July, and August between 35°N and 60°N . However, at latitudes north of 60°N , NDVI peaks only in the months of July and August (Figure 7), thus indicating a shorter growing season. For the time being, the May to September definition will suffice; changes in both the amplitude and the actual growing season duration are discussed separately below. Moreover, the average, rather than the total, May to September NDVI is discussed, for they differ only by a constant.

The time series of monthly NDVI anomaly totals for 5° latitude bands between 35°N and 70°N are shown in Figures 8a and 8b for the east and west quadrants, respectively. The upward trend in anomalies is seen at all latitudes over the entire period of record. The May to September average NDVI at these latitudes in each of the two quadrants is shown in Figures 9a and 9b. A statistically significant increase in seasonal green-

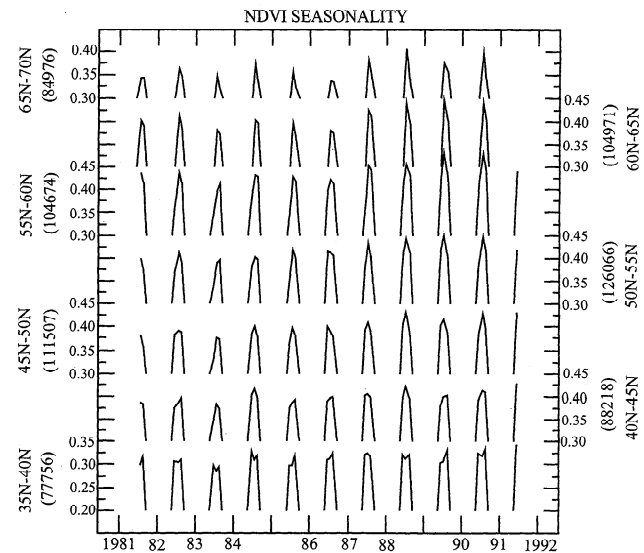


Figure 7. Temporal profiles of NDVI during the boreal summer months of June, July, and August for various 5° latitudinal bands. The number of vegetated pixels during August is also shown in parentheses.

ness is seen everywhere, with the exception of the 40°N – 45°N latitudinal band in the western quadrant. About 47% of the total vegetated area in the month of August is contained in these two quadrants (29 and 18%). The overall increase in greenness amounts to about 13%, with the eastern quadrant showing a slight higher increase than the western quadrant (14 versus 12%). The most significant increase is seen, however, in areas north of 50°N latitude: 16% over an area that is about 28% of the total vegetated area in August. The western quadrant shows a higher increase (18%) than the eastern quadrant (15%), but the latter is almost twice as large in terms of vegetated area during the boreal summer (18%).

Because of their high spatial resolution, relative to ground-based meteorological measurements, NDVI data provide spatial detail of where the average changes in amplitude and timing of the active growing season occurred. To address regional variations in NDVI, we show in Plate 1a, a map related to the time plots shown in Figures 9a and 9b, together with a map of the 9 year average of NDVI for comparison (Plate 1b).

The linear rate of change in NDVI, averaged over the 9 years of seasonal NDVI data in northern latitudes, from 1982 to 1990, are mapped in Plate 1a. Data were averaged from May to September to approximate the main active growing season of land vegetation in the northern hemisphere. In Eurasia a band of increasing NDVI extends from Spain in a northeasterly direction across Asia to the western Pacific Ocean. In this band, central Europe, southern Russia, and a broad region near Lake Baikal in Siberia are most affected. Outside this band, northern Scandinavia, northern China, and northeastern Siberia are also strongly affected. In North America a band of increasing NDVI extends from Alaska in a southeasterly direction to the Great Lakes, then northeasterly to Labrador. In this band, northwestern Canada is most strongly affected. Outside of this band, the continental United States, exclusive of Alaska, and the area around the Hudson Bay show little change in NDVI.

In general, the regions of greatest increase in NDVI are inland from the oceans, except in the Arctic, and are north of

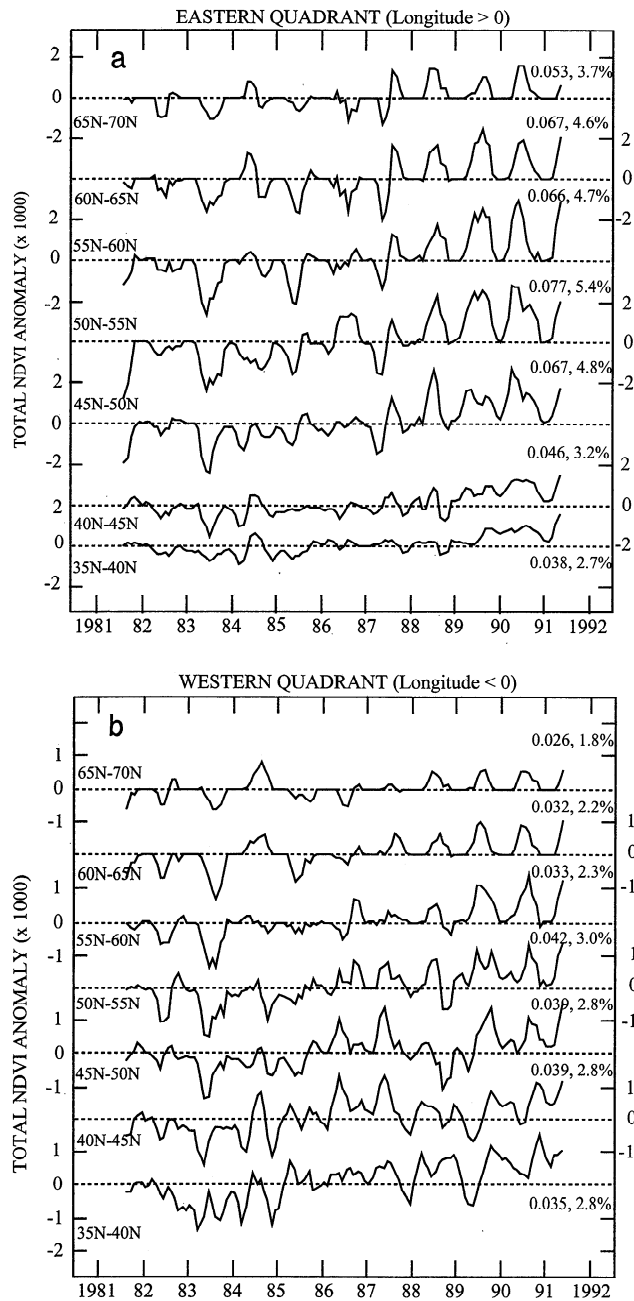


Figure 8. Time series of spatial sums of monthly NDVI anomalies in various 5° latitudinal bands in (a) eastern and (b) western quadrants. The two numbers for each band shown in this figure are (1) the number of vegetated pixels in August (in millions) and (2) the fractional contribution to total vegetated area of the globe during August (as percent).

50°N. The prominent bands of increased NDVI, referred to above in both Eurasia and North America, correspond generally to areas of high NDVI (Plate 1b). Thus most of the areas where changes in NDVI amplitude and seasonality were observed are also regions of significant vegetation density. Notable exceptions are several Arctic regions in Eurasia where NDVI rose sharply from low initial values.

5.2. Seasonal NDVI Amplitude

The time series of monthly NDVI, when spatially averaged over coarse latitudinal bands (Figure 5a), indicate that the

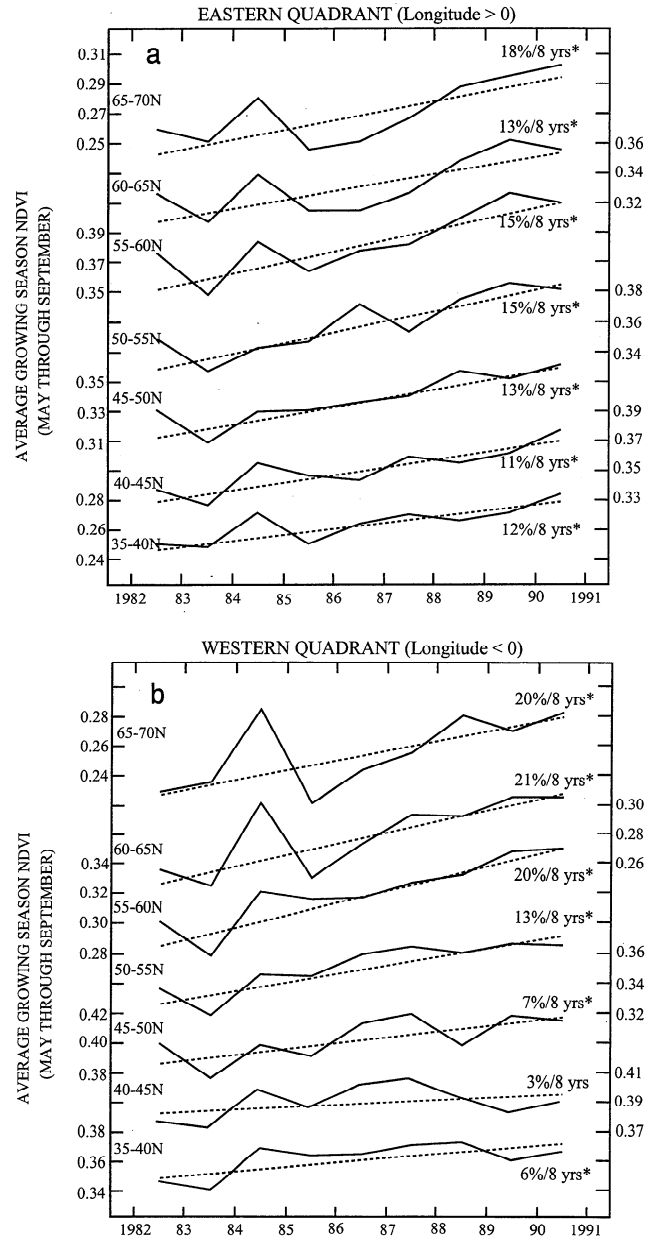


Figure 9. Average May to September NDVI of 5° latitudinal bands in (a) eastern and (b) western quadrants. Statistically significant (>10%) linear trend estimates are marked with an asterisk.

wintertime NDVI is close to zero in the northern high latitudes. Therefore the summer time peak NDVI values can be regarded as the seasonal amplitudes of NDVI. While this definition is valid at latitudes north of 45°N, it introduces a slight inaccuracy at latitudes between 30°N and 45°N, because the wintertime NDVI there is about 0.05 (Figure 5a). This value does not change appreciably from year to year and can therefore be viewed as an offset that must be subtracted from the peak summertime NDVI value to obtain the amplitude. This must be kept in mind when NDVI amplitude results for the 35°N–40°N and 40°N–45°N latitudinal bands are presented below, for such an offset correction has not been made; however, this has no impact on the inferences drawn.

Seasonal NDVI amplitude at latitudes north of 35°N is

HIGH LATITUDE GREENING TREND (1982–1991)

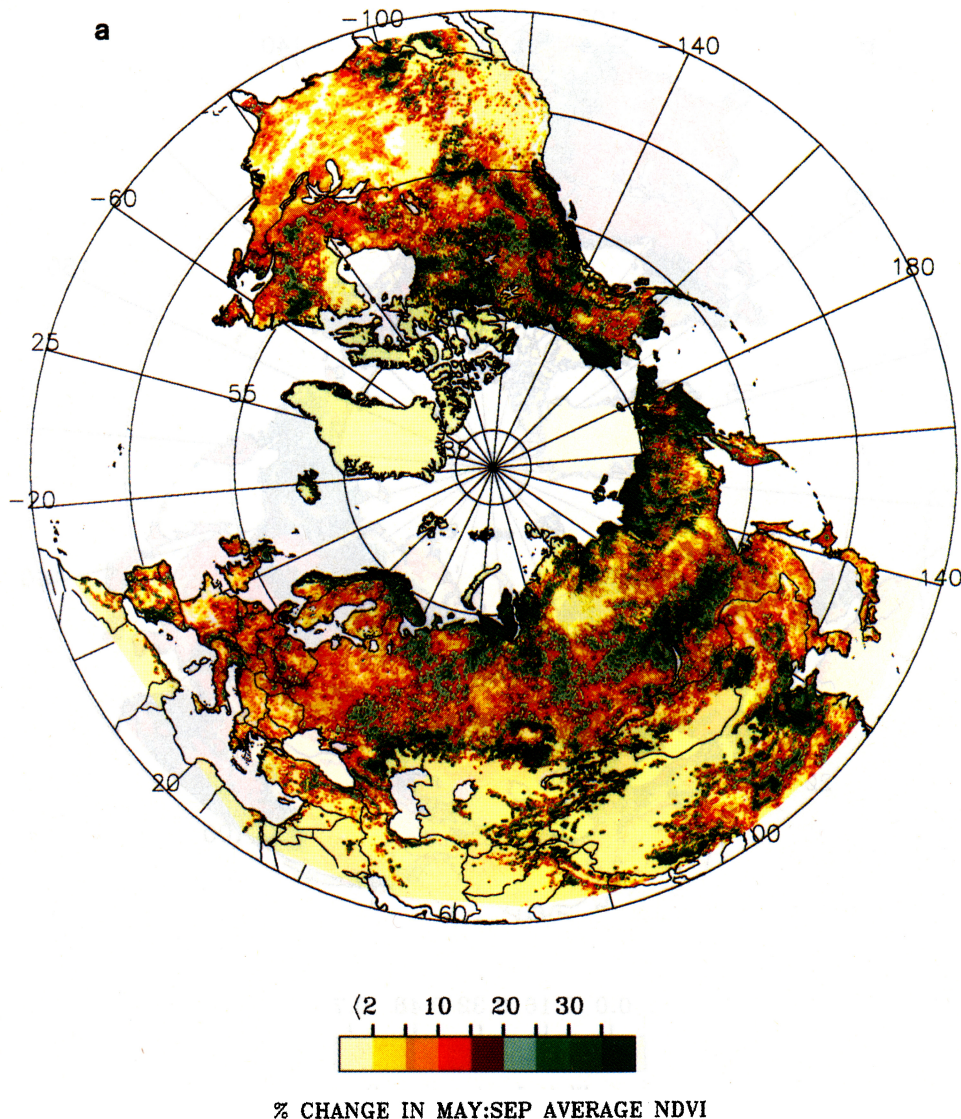


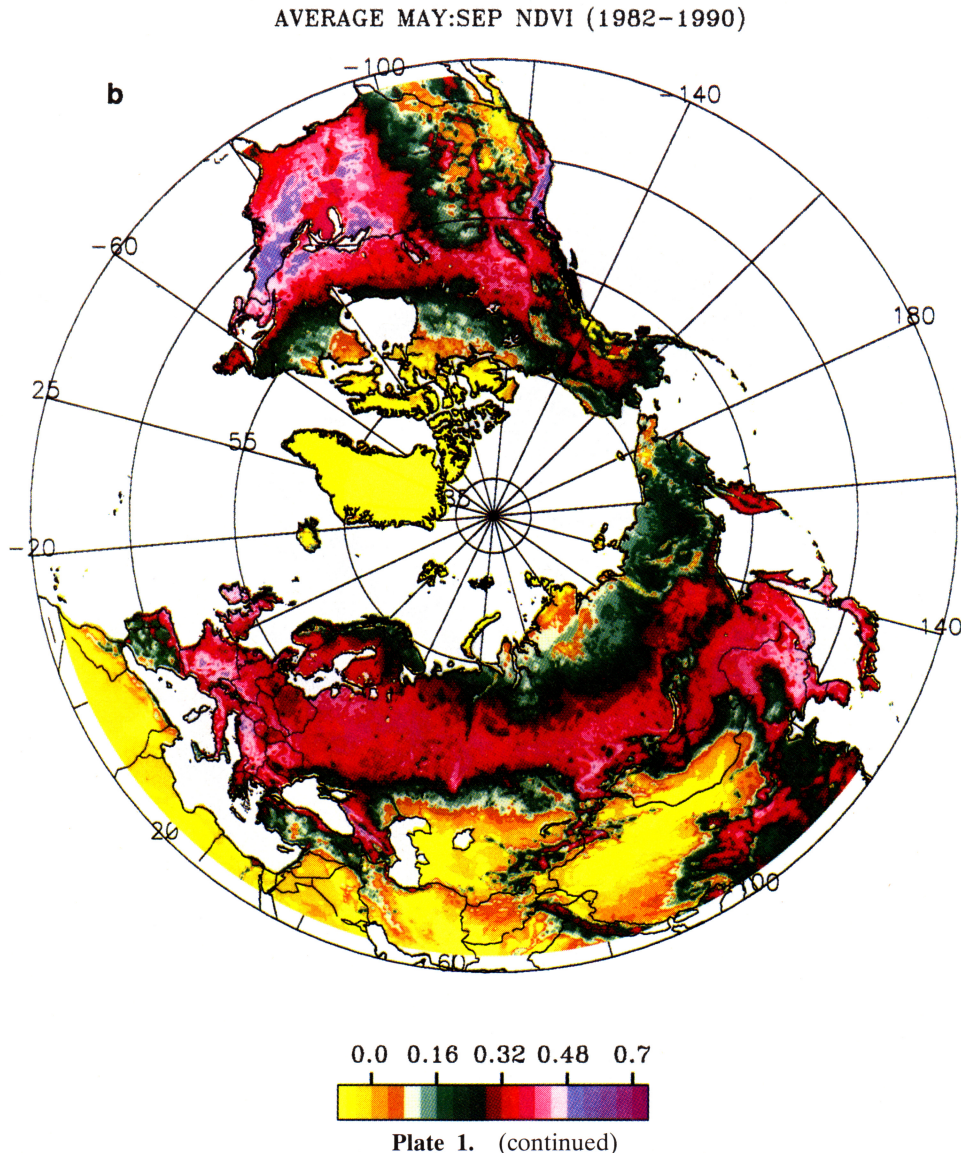
Plate 1. (a) Color-coded contour plot of statistically significant increase in May to September average NDVI for areas north of 27.75° . (b) Color-coded contour plot of May to September average NDVI for areas north of 27.75° .

shown in Figure 10a. Results from both the Pathfinder (left ordinate) and the GIMMS (right ordinate) NDVI data sets are shown together with the corresponding rates of increase. The seasonal amplitude, by the above definition, increased by 7 to 14%, depending on the latitude and data set, from 1981 or 1982 through 1990 (Figure 10a). Because NDVI is a measure of photosynthetic activity of vegetation as noted earlier, this increase indicates a substantial change in photosynthetic activity of plants at higher northern latitudes. A similar increase (14%) is indicated (Figure 10b) in the amplitude of the seasonal cycle of atmospheric CO_2 measured at Point Barrow, Alaska [Keeling *et al.*, 1996]. This CO_2 cycle, although observed in the Arctic (71°N), registers changes in CO_2 gas exchanges and hence in the biotic activity of plants and soil over all northern temperate and polar latitudes [Heimann *et al.*, 1989]. Together, the NDVI and CO_2 data indicate increased biospheric activity north of about 35°N . Two recent studies have also reported increased photosynthetic activity in the northern

high latitudes as increased biomass from deposition in European forests [Kauppi *et al.*, 1992] and from tree-ring analysis in Mongolia [Jacoby *et al.*, 1996].

The NDVI amplitude trend in the northern high latitudes shown in Figure 10a needs to be discussed in light of known problems with the NDVI data sets. For instance, a question arises about the effect of stratospheric aerosols on NDVI due to the eruption of El Chichón in April 1982, as both Pathfinder and GIMMS data set have no explicit corrections for these effects. We found that the eruption of El Chichón had no appreciable effect on NDVI data from latitudes north of about 40°N for the following reasons:

1. The time series of calibrated NDVI from both the Pathfinder and the GIMMS data sets do not show an anomalous decline in NDVI (Figures 5a and 5b).
2. The seasonal NDVI amplitude actually shows an increase from 1981 to 1982, rather than a decrease (Figure 10a). The International Satellite Cloud Climatology Project



(ISCCP) processing of AVHRR data discards 10 months of data from June 1982 to March 1983 because of El Chichón effects (W. L. Rossow, personal communication, 1997). Had the high-latitude data been corrupted, we would not expect an increase in NDVI amplitude from 1981 to 1982, unless, of course, if 1982 had been an exceptionally congenial year for vegetation growth, and the real increase was much larger than that observed because of El Chichón effects. At least from temperature data we can conclude that this was perhaps not the case, because the 50°N–80°N thermometer temperature data actually show a decrease from 1981 to 1982 [Keeling *et al.*, 1996].

3. On the basis of ISCCP processing, the 1983 amplitude must be free of El Chichón effects. The decline in 1983, seen in both data sets, matches well with the trend in the relative amplitude of atmospheric CO₂ measured at Point Barrow (Figure 10b). Therefore this decline is likely due to climate and not due to El Chichón effects.

4. The increase in amplitude from 1983 to 1984, seen in both Pathfinder and GIMMS data, also matches the trend in atmospheric CO₂ concentration. Importantly, the trend from

1981 to 1984 is counterintuitive to what it should be, had there been significant El Chichón effects in NDVI data.

Could the observed greening trend in the high latitudes be an artifact due to residual intersensor variations? We provide below arguments why the greening trend is not an artifact.

1. The trend is best seen in NDVI anomalies (Figures 8a and 8b) and seasonal NDVI amplitudes (Figures 9a, 9b, and 10a). We argued above that the data from the NOAA 7 period are free of significant El Chichón-related effects. The data from the NOAA 9 period, from February 1985 to October 1988, also show an upward trend. The NDVI amplitude in 1988 (NOAA 9) is already high, having begun increasing in 1987, and is comparable to the amplitude observed in 1989, the first year of NOAA 11 data.

2. Assume that the trend in NDVI amplitude north of 45°N is an artifact. We can detrend the data by revising the individual calibration factors (note that these are multiplicative). These “new” channel, instrument, and time-dependent calibration factors can now be used to derive the time series of Saharan NDVI, a nonvegetated invariant target, in order to assess whether the high-latitude greening trend is an instru-

mental artifact or not. This has been done with the GIMMS data. When the high-latitude trend is removed, the resulting time series for the Sahara shows a decreasing trend, which is unrealistic.

3. One could argue that latitude-dependent artifacts, due to Sun angle changes, disallow such exercises. Indeed, NDVI variations due to intra-annual (seasonal) and interannual (orbital drift) Sun angle changes have not been corrected for in either of the two data sets. However, such variations are small if we confine our analysis to a fixed time of the year (July and August, say) and to the initial years of satellite launch, when orbital drift is minimal (1981–1982 for NOAA 7, 1985–1986 for NOAA 9, and 1989–1990 for NOAA 11). Figure 10a (and Figures 9a and 9b) shows that the NDVI data from these periods exhibited an increasing trend.

4. The warming trend observed in near-surface air temperatures during the 1980s peaked in the 1989–1990 time period, which seems to substantiate the observed increase in the seasonal amplitude of atmospheric CO₂ concentration [Keeling *et al.*, 1996]. The decrease in snow cover extent in the high latitudes has also been documented and the feedback effect of albedo on temperature quantified [Groisman *et al.*, 1994a, b]. The geographical distribution of the high-latitude greening trend observed in the NDVI data (Plate 1a) matches well with the pattern of springtime warming deduced from thermometer data [Chapman and Walsh, 1993]. The totality of this evidence argues against the trend in NDVI being an artifact.

5.3. Growing Season Length

An estimate of growing season length requires precise determination of the timing of spring green-up and autumn leaf fall. The timing of these two events may be defined in terms of NDVI data. It will be recalled that Pathfinder NDVI data are a 10-day maximum-value composite; that is, the maximum NDVI value during a 10 day period is used to represent the NDVI during those 10 days. In the following analysis the 10 day composite NDVI value was assigned to day 5 of the corresponding compositing period. There were three such approximate 10 day compositing periods per month, as described earlier. The temporal profile of NDVI was evaluated for each 8 km Pathfinder pixel and then spatially averaged according to method A described earlier. This analysis was done for all years from 1982 to 1990. The yearly temporal profiles were then averaged over two consecutive years (1982–1983, 1985–1986, 1987–1988, and 1989–1990). These profiles are shown together with a 10 day average station temperature slope profile during the same period (Figures 11a and 11b).

The rise in NDVI, spatially averaged from 45°N to the northern limit of the data, came progressively earlier in the season between 1982 and 1990, as shown by successive 10 day averages, where each plot shows an average over two years for clarity. Because spatially averaged NDVI rose each year at nearly a constant rate from early April (about day 110) to late June (about day 170), the advance in the growing season is apparent, notwithstanding the relatively coarse (10 days) time resolution afforded by the Pathfinder NDVI data. From six estimates of the advance at successive thresholds of NDVI, we estimate an advance of 8 ± 3 days.

An advance of about 7 days in the seasonal cycle was previously inferred from atmospheric CO₂ data as having taken place between the 1960s and the early 1990s, with most of the increase occurring after 1980 [Keeling *et al.*, 1996, Figure 1]. The NDVI data demonstrate that this increase occurred over

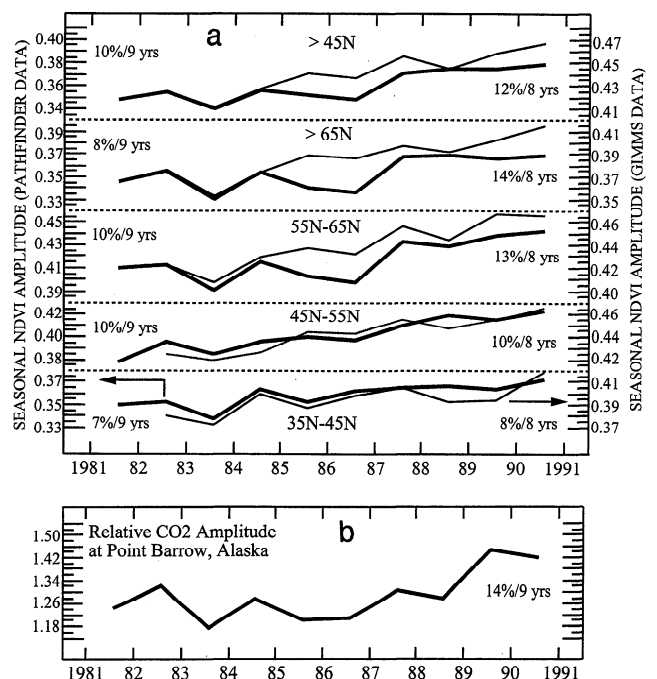


Figure 10. Seasonal NDVI amplitude in the northern high latitudes (a) compared to the amplitude of atmospheric CO₂ (b) measured at Point Barrow, Alaska [Keeling *et al.*, 1996]. Statistically significant (>10%) linear trend estimates are marked with an asterisk.

an extensive region of the extratropical northern hemisphere. The Pathfinder NDVI data in Figure 11a further show a prolongation of the declining phase of the growing season, estimated at 4 ± 2 days between 1982–1983 and 1989–1990. Therefore the growing season north of 45°N appears to have lengthened by 12 ± 4 days over the 1980s. These estimates must be interpreted as suggestive of a longer active growing season, rather than in an absolute sense, in view of the coarse temporal resolution (10 days) and residual atmospheric effects in NDVI data. The associated standard errors given here are not rigorous, for low-frequency variations in NDVI data invalidate the assumption of statistical independence required of the successive threshold values.

Variations in the amplitude and timing of the seasonal cycle of atmospheric CO₂ have shown an association with surface air temperature consistent with the hypothesis that warmer temperatures have promoted increases in plant growth outside the tropics. A likely cause is an increase in the length of the growing season brought about by warmer temperatures [Keeling *et al.*, 1996]. As shown in Figure 11b, a pronounced increase in late winter and early spring temperatures took place over the period of NDVI changes, especially during March.

5.3.1. Latitudinal analysis. The above analysis included all pixels north of 45°N. It is of some interest to investigate if the observed changes in growing season length have a latitudinal dependence. Moreover, the analysis can be somewhat refined by (1) investigating only those pixels that exhibit seasonality, i.e., excluding pixels of evergreen (needle) vegetation and (2) using a different method of evaluating changes in growing season length. Data from April to October were first aggregated from their native 8×8 km resolution to a $0.25^\circ \times 0.25^\circ$ resolution. Results presented in this section were derived from this equal angle data set to reduce computational burden.

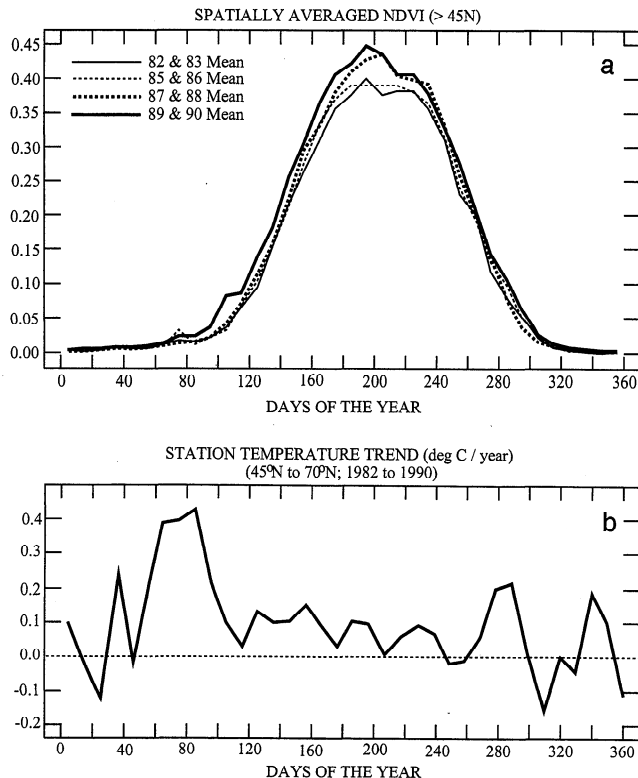


Figure 11. (a) Temporal profile of NDVI spatially averaged according to method A described in the text for all pixels north of 45°N. The difference between the 1982–1983 and 1989–1990 biyearly average profiles can be translated into an estimate of the changes in growing season length as described in the text. (b) Changes in the annual cycle of near-surface air temperature from 1982 to 1990. Daily thermometer observations of maximum and minimum temperatures were averaged to obtain daily temperatures and interpolated on a $1^\circ \times 1^\circ$ grid [Piper and Stewart, 1996]. The daily data were further averaged over three approximately 10 day periods per month to obtain 36 observations per year. The 10 day average temperatures were then regressed on the year (1982 to 1990) to obtain the slopes shown here.

5.3.2. Seasonality characterization. Monthly NDVI was calculated as the average of three 10 day composites in a month and assigned to day 15 of the month. Let $y(5)$ be the pixel NDVI in May, $y(6)$ the NDVI in June, and so on. The following criteria were used to determine seasonality from NDVI time series of each quarter degree pixel: (1) $y(5), y(6), \dots, y(9) > 0.0$; (2) $y(5) < y(6)$ and $y(8) > y(9)$; (3) seasonal NDVI amplitude Y defined as $[y(7) + y(8)]/2$ must be greater than 0.35; and (4) $Y > 1.25 \times y(5)$ and $Y > 1.25 \times y(9)$. These conditions ensure that pixels with missing values and evergreen land covers are not included in the analysis on growing season.

There are 117,601 quarter degree land pixels between 35°N and 70°N latitudes. The distribution of these pixels and the fraction that exhibit seasonality, i.e., those that satisfy the above mentioned criteria, changes with latitude: (1) 26,185 land pixels between 35°N and 45°N, with 6.5% of these exhibiting seasonality; (2) 33,264 and 30.7% between 45°N and 55°N; (3) 36,400 and 44.7% between 55°N and 65°N; (4) 21,752 and 17% between 65°N and 70°N, and (5) 91,416 and 33%

between 45°N and 70°N. These numbers must be kept in mind when discussing the following results.

5.3.3. Growing season duration. The length of growing season at a location can be evaluated from the time series of NDVI data with a method developed and refined by Bhadwar [1984b]. This method was first developed to estimate agricultural crop emergence dates from spectral reflectance data [Bhadwar, 1980]. The method was later successfully used to classify Landsat data scenes for the estimation of crop extent [Bhadwar et al., 1982; Bhadwar, 1984a; Bhadwar and Henderson, 1985]. The method used in this study is described by Bhadwar [1984b]. It involves fitting the following function:

$$y(x) = a(x/b)^p \exp [q(b^2 - x^2)]$$

to the temporal profile of NDVI data to estimate the four coefficients a , b , p , and q . If y is NDVI at time x , number of days since January 1, the coefficients a and b have physical meaning: NDVI before spring green-up and date of spring green-up, respectively. This significance is not invoked in this analysis because of coarse temporal and spatial resolution of satellite data, and the four coefficients are treated as such. It is of some interest to note that the above function is a special case of Weibull distribution: {Let $z = \sqrt{qx}$; then $y(z) = cz^p \exp(-z^2)$, with $c = [a \exp(b^2q)]/[b^p q^{p/2}]$. Thus Weibull's $\gamma = 0$, Weibull's $\alpha = 2/(p + 1)$, and Weibull's $\beta = p + 1$ }. The Weibull distribution is skewed to the right for all values of the parameters. However, the skewness decreases as the shape parameter (Weibull's β) increases. In fact, it can be shown that for some combination of the parameters ($\alpha = 1$, $\beta = 3.2589$, and $\gamma = 0$), the Weibull density is identical to the Gaussian density ($\mu = 0.8964$, $\sigma = 0.0924$) [Tsokos, 1972, page 181].

The temporal profile of monthly NDVI data from April to October was fitted to the above mentioned function, and the number of days with NDVI greater than a threshold value was estimated from the fitted profile, pixel by pixel. The growing season length, thus estimated, is dependent on the threshold NDVI value. Therefore it is important to assess the sensitivity of the change in growing season length to NDVI threshold. The results are shown in Figure 12a, for the 50°N–60°N latitudinal band in the eastern quadrant, where a significant increase in growing season NDVI (15%) was observed (Figure 9a), and which constitutes slightly more than 10% of the global vegetated area in August. It can be seen that the change in growing season length (8 days from 1982 to 1990) is nearly invariant of NDVI threshold values between 0.1 and 0.35. Further confirmation of this can be visually had from Figures 11a, where the difference in NDVI profiles between the early (1982 and 1983) and the later (1989 & 1990) years of the 1980s is seen to be nearly invariant of the NDVI threshold. Therefore a threshold value of 0.25 NDVI was used in further analysis.

Growing season lengths thus estimated for all quarter degree pixels, which satisfied the above mentioned seasonality criteria, were spatially averaged to obtain latitudinal measures. Results for latitudes between 35°N and 70°N are shown in Figure 12b, together with the timing of the midpoint in the drawdown of CO_2 between spring and summer at Point Barrow, Alaska [cf. Keeling et al., 1996]. Linear trend estimates of the change in growing season duration are also shown; statistically significant estimates are marked with an asterisk. It appears that at latitudes north of 45°N the number of days with NDVI greater than 0.25 increased by about 9 days from 1982 to 1990. This estimate is comparable to the 7 day advance

observed in the timing of midpoint of CO₂ drawdown between spring and summer at Point Barrow for the same time period [Keeling *et al.*, 1996] and is within the range (12 ± 4 days) obtained above (compare Figure 11a) when all pixels north of 45°N were included in the analysis. A slightly larger increase in growing season length (10 days) is observed at latitudes between 55°N and 70°N.

Some discussion on the reliability of these results is relevant here. This is done in the context of the 55°N–65°N latitudinal band, as an example. There are 36,400 quarter degree pixels on land in this latitudinal band. About 40% of these pixels satisfy the seasonality criteria noted above. This number varies from year to year, with a minimum in 1985 (36%) and a maximum in 1990 (45%). The goodness of fit, evaluated as the square root of mean sum of squared differences between the measured and the fitted NDVI values (April to October, $N = 7$), is on an average about 0.04 NDVI. The average number of days with NDVI > 0.25 increased from about 109 days in 1982 to about 117 days in 1990. The standard deviations σ are typically about 15 days, indicating a large variation in the growing season length within this latitudinal band. The standard deviation of the mean growing season, evaluated as $\sigma/\sqrt{N_p}$, is quite small, indicating that the estimated mean is a reliable indicator of the true mean (because N_p is so large), and that the ability to distinguish between average growing season duration between years, the result sought here, can be done reliably.

6. Concluding Remarks

The key findings can be summarized as follows: (1) satellite-sensed vegetation index averaged over the boreal growing season months of May to September increased by about 13% from 1982 to 1990 (8 years) at latitudes north of 35°N, (2) the seasonal amplitude of this index increased by about 10% from 1981 to 1990 (9 years) at latitudes north of 45°N, and (3) the timing of spring green-up advanced by about 8 ± 3 days between 1982 and 1990 at latitudes between 45°N and 70°N to result in a lengthening of the growing season by about 12 ± 4 days.

Analyses of station temperature trends during 1961–1990 indicate pronounced warming over substantial areas in Alaska, northwestern Canada, and northern Eurasia [Chapman and Walsh, 1993]. The greatest warming, up to 4°C, has occurred in winter. Only slightly lesser warming has occurred in the same regions in spring but considerably lesser warming in summer and even less in autumn. Associated with warming at high latitudes is an approximate 10% reduction in annual snow cover from 1973 to 1992, especially an earlier disappearance of snow in spring [Groisman *et al.*, 1994a, b, Table 1]. Where snow lines have retreated earlier due to enhanced warming, we expect an early start of the active growing season. The geographical distribution of the increase in NDVI matches well with the springtime warming pattern.

The winter and spring warming in the interior of the continents of Asia and North America in the 1980s may be a result of natural causes not yet explained, but its timing is consistent with an enhanced greenhouse effect caused by buildup of infrared-absorbing gases in the atmosphere [Intergovernmental Panel on Climate Change (IPCC), 1995]. The unusual warming which peaked near 1990 was of global extent. Although it amounted to only a few tenths of a degree departure from previous record temperatures [Jones *et al.*, 1994], it was associated with far greater warming in the spring months at high

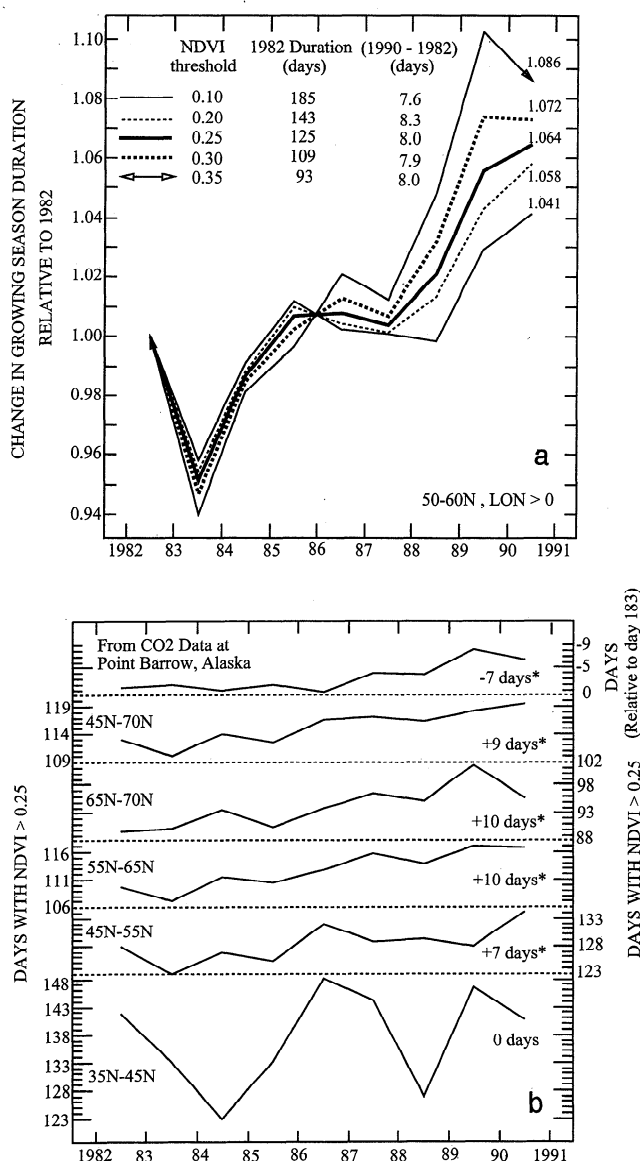


Figure 12. (a) Sensitivity of the change in the number of days with NDVI > 0.25 to NDVI threshold values between 0.1 and 0.35. (b) Change in growing season duration, defined as the number of days with NDVI > 0.25, during the 1980s. The advance in the midpoint of the drawdown of atmospheric CO₂ at Point Barrow, Alaska [Keeling *et al.*, 1996], is shown at the top. Statistically significant (>10%) linear trend estimates are marked with an asterisk.

northern latitudes. Biospheric activity there, based on our analysis, increased remarkably as a result of this warming, suggesting that small changes in global temperature may reflect disproportionate responses at the regional level and may be accompanied by positive feedbacks that can markedly influence processes such as photosynthesis and litter decomposition.

Acknowledgments. This research was supported in part by the Terrestrial Ecology program of NASA, NASA EOS-AM platform instruments (MODIS and MISR) science team funds, Electric Power Research Institute, and the U.S. National Science Foundation. We gratefully acknowledge contributions to this research by S. Nicholson (rainfall data), Whorf (CO₂-related data in Figures 6 and 11), Piper

and Stewart (temperature results in Figure 151, top panel). We are grateful to these key contributions. We also thank S. Kalluri and P. Smith of the AVHRR Land Pathfinder program for valuable discussions.

References

- Agbu, P. A., and M. E. James, *The NOAA/NASA Pathfinder AVHRR Land Data Set User's Manual*, Goddard Distrib. Activ. Arch. Cent., NASA Goddard Space Flight Cent., Greenbelt, Md., 1994.
- Alexander, M. A., and K. M., Weickmann, Biennial variability in an atmospheric general circulation model, *J. Clim.*, **8**, 431–440, 1995.
- Anonymous, *World Climate News*, vol. 9, 1996.
- Asrar, G., M. Fuchs, E. T. Kanemasu, and J. L. Hatfield, Estimating absorbed photosynthetic radiation and leaf area index from spectral reflectance in wheat, *Agron. J.*, **76**, 300–306, 1984.
- Badhwar, G. D., Crop emergence date determination from spectral data, *Photogr. Eng. Remote Sens.*, **46**, 369–377, 1980.
- Badhwar, G. D., Automatic corn-soybean classification using LANDSAT MSS data, I, Near-harvest crop proportion estimation, *Remote Sens. Environ.*, **14**, 15–29, 1984a.
- Badhwar, G. D., Use of LANDSAT-derived profile features for spring small-grains classification, *Int. J. Remote Sens.*, **5**, 783–797, 1984b.
- Badhwar, G. D., and K. E. Henderson, Application of Thematic Mapper data to corn and soybean development stage estimation, *Remote Sens. Environ.*, **17**, 197–201, 1985.
- Badhwar, G. D., W. W. Austin, and J. G. Carnes, A semi-automatic technique for multitemporal classification of a given crop within a landscape scene, *Pattern Recognition*, **15**, 217–230, 1982.
- Chapman, W. L., and J. E. Walsh, Recent variations of sea ice and air temperatures in high latitudes, *Bull. Am. Meteorol. Soc.*, **74**, 33–47, 1993.
- Fung, I. Y., C. J. Tucker, and K. C. Prentice, Application of advanced very high resolution radiometer vegetation index to study atmosphere-biosphere exchange of CO₂, *J. Geophys. Res.*, **92**, 2999–3015, 1987.
- Groisman, P. Y., T. R. Karl, and R. W. Knight, Observed impact of snow cover on the heat balance and the rise of continental spring temperatures, *Science*, **263**, 198–200, 1994a.
- Groisman, P. Y., T. R. Karl, and R. W. Knight, Changes of snow cover, temperature, and radiative heat balance over the northern hemisphere, *J. Clim.*, **7**, 1633–1656, 1994b.
- Heimann, M., C. D. Keeling, and C. J. Tucker, A Three-dimensional model of atmospheric CO₂ transport based on observed winds, 3, Seasonal cycle and synoptic timescale variations, in *Aspects of Climate Variability in the Pacific and Western Americas*, *Geophys. Monogr. Ser.*, vol. 55, edited by D. H. Peterson, pp. 277–303, AGU, Washington, D. C., 1989.
- Holben, B. N., Characteristics of maximum value composite images for temporal AVHRR data, *Int. J. Remote Sens.*, **7**, 1417–1437, 1986.
- Intergovernmental Panel on Climate Change (IPCC), *Climate Change 1995*, edited by J. T. Houghton, L. G. Meira Filho, B. A. Callander, N. Harris, A. Kattenberg, and K. Maskell, 572 pp., Cambridge University Press, New York, 1995.
- Jacoby, G. C., R. D'Arrigo, and T. Davaajamts, Mongolian tree rings and 20th-century warming, *Science*, **273**, 771–773, 1996.
- James, M. F., and S. N. V. Kalluri, The Pathfinder AVHRR land data set: An improved coarse-resolution data set for terrestrial monitoring, *Int. J. Remote Sens.*, **15**, 3347–3364, 1994.
- Jones, P. D., T. M. L. Wigley, and K. R. Briffa, Global and hemispheric temperature anomalies—Land and marine instrumental records, in *Trends '93: A Compendium of Data on Global Change*, edited by T. A. Boden, D. P. Kaiser, R. J. Sepanski, and F. W. Stoss, pp. 603–608, *ORNL/CDIAC-65*, Carbon Dioxide Inf. Anal. Cent., Oak Ridge Natl. Lab., Oak Ridge, Tenn., 1994.
- Kauppi, P. E., K. Mieliäinen, and K. Kuusela, Biomass and carbon budget of European forests from 1971–1990, *Science*, **256**, 70–74, 1992.
- Keeling, C. D., T. P. Whorf, M. Wahlen, and J. van der Plicht, Interannual extremes in the rate of rise of atmospheric carbon dioxide since 1980, *Nature*, **375**, 666–670, 1995.
- Keeling, C. D., J. F. S. Chin, and T. P. Whorf, Increased activity of northern vegetation inferred from atmospheric CO₂ measurements, *Nature*, **382**, 146–149, 1996.
- Loeb, N. G., In-flight calibration of NOAA AVHRR visible and near-IR bands Greenland and Antarctica, *Int. J. Remote Sens.*, **18**, 477–490, 1997.
- Myneni, R. B., F. G. Hall, P. J. Sellers, and A. L. Marshak, The interpretation of spectral vegetation indexes, *IEEE Trans. Geosci. Remote Sens.*, **33**, 481–486, 1995.
- Myneni, R. B., S. O. Los, and C. J. Tucker, Satellite-based identification of linked vegetation index and sea surface temperature anomaly areas from 1982–1990 for Africa, Australia and South America, *Geophys. Res. Lett.*, **23**, 729–732, 1996.
- Philander, S. G. H., *El Niño, La Niña, and the Southern Oscillation*, Academic, San Diego, Calif., 1990.
- Piper, S. C., and E. F. Stewart, A gridded global data set of daily temperature and precipitation for terrestrial biosphere modeling, *Global Biogeochem. Cycles*, **10**(4), 757–782, 1996.
- Price, J., Timing of the NOAA afternoon passes, *Int. J. Remote Sens.*, **12**, 193–198, 1991.
- Prince, S. D., A model of regional primary production for use with coarse resolution satellite data, *Int. J. Remote Sens.*, **12**, 1313–1330, 1991.
- Rao, C. R. N., and J. Chen, Inter-satellite calibration linkages for the visible and near-infrared channels of the Advanced Very High Resolution Radiometer on the NOAA-7, -9, and -11 spacecraft, *Int. J. Remote Sens.*, **16**, 1931–1942, 1995.
- Tanrè, D., B. N. Holben, and Y. J. Kaufman, Atmospheric correction algorithm for NOAA-AVHRR products: Theory and application, *IEEE Trans. Geosci. Remote Sens.*, **30**, 231–248, 1992.
- Thomson, D. J., The seasons, global temperature, and precession, *Science*, **268**, 59–68, 1995.
- Tsokos, C. P., *Probability Distributions: An Introduction to Probability Theory With Applications*, Duxbury, Boston, Mass., 1972.
- Tucker, C. J., A critical review of remote sensing and other methods for nondestructive estimation of standing crop biomass, *Grass Forage Sci.*, **35**, 177–182, 1980.
- Tucker, C. J., History of the use of AVHRR data for land applications, in *Advances in the Use of NOAA AVHRR Data for Land Applications*, edited by G. D'Souza, pp. 1–19, Eur. Econ. Community, Brussels, 1996.
- Tucker, C. J., J. R. G. Townshend, and T. E. Goff, African land-cover classification using satellite data, *Science*, **227**, 369–375, 1985.
- Tucker, C. J., I. Y. Fung, C. D. Keeling, and R. H. Gammon, Relationship between atmospheric CO₂ variations and a satellite-derived vegetation index, *Nature*, **319**, 195–199, 1986.
- Tucker, C. J., H. E. Dregne, and W. W. Newcomb, Expansion and contraction of the Saharan desert from 1980 to 1990, *Science*, **253**, 299–301, 1991.
- Tucker, C. J., W. W. Newcomb, and H. E. Dregne, AVHRR data sets for determination of desert spatial extent, *Int. J. Remote Sens.*, **15**, 3547–3565, 1994.
- Voss, R. S., R. L. Schmoyer, P. M. Steurer, T. C. Peterson, R. Heim, T. R. Karl, and J. K. Eischeid, *The Global Historical Climatology Network: Long-term Monthly Temperature, Precipitation, Sea Level Pressure and Station Pressure Data*, Carbon-Dioxide Inf. Anal. Cent., Oak Ridge Natl. Lab., Oak Ridge, Tenn., 1992.
- Woddruff, S. D., et al., *Comprehensive Ocean-Atmosphere Data Set (COADS) Release 1a: 1980–1992*, Natl. Oceanic and Atmos. Admin., Washington, D. C., 1993.
- G. Asrar, Mission to Planet Earth, NASA Headquarters, Code SE, Washington, D. C. 20546.
- C. D. Keeling, Scripps Institute of Oceanography, La Jolla, CA 92093.
- R. B. Myneni, Department of Geography, 675 Commonwealth Avenue, Boston University, Boston, MA 02215-1401. (e-mail: rmyneni@crsa.bu.edu)
- C. J. Tucker, Biospheric Sciences Branch, NASA Goddard Space Flight Center, Greenbelt, MD 20771.

(Received March 14, 1997; revised December 2, 1997; accepted December 3, 1997.)